doi:10.1093/brain/aws286 Brain 2013: 136; 65–80 | 65

BRAIN
A JOURNAL OF NEUROLOGY

Antagonism of purinergic signalling improves recovery from traumatic brain injury

Anthony M. Choo,[1,*] William J. Miller,[1,*] Yung-Chia Chen,[1] Philip Nibley,[1] Tapan P. Patel,[1] Cezar Goletiani,[2] Barclay Morrison III,[2] Melinda K. Kutzing,[3] Bonnie L. Firestein,[3] Jai-Yoon Sul,[4] Philip G. Haydon[5] and David F. Meaney[1]

1 Department of Bioengineering, University of Pennsylvania, Philadelphia, PA, USA
2 Department of Biomedical Engineering, Columbia University, New York, NY, USA
3 Department of Cell Biology and Neuroscience, Rutgers University, Piscataway, NJ, USA
4 Department of Pharmacology, University of Pennsylvania, Philadelphia, PA, USA
5 Department of Neuroscience, Tufts University, Boston, MA, USA

*These authors contributed equally to this work.

Correspondence to: David F. Meaney,
Department of Bioengineering,
Suite 240 Skirkanich Hall,
210 South 33rd Street,
Philadelphia, PA 19104-6321, USA
E-mail: dmeaney@seas.upenn.edu

The recent public awareness of the incidence and possible long-term consequences of traumatic brain injury only heightens the need to develop effective approaches for treating this neurological disease. In this report, we identify a new therapeutic target for traumatic brain injury by studying the role of astrocytes, rather than neurons, after neurotrauma. We use *in vivo* multiphoton imaging and show that mechanical forces during trauma trigger intercellular calcium waves throughout the astrocytes, and these waves are mediated by purinergic signalling. Subsequent *in vitro* screening shows that astrocyte signalling through the 'mechanical penumbra' affects the activity of neural circuits distant from the injury epicentre, and a reduction in the intercellular calcium waves within astrocytes restores neural activity after injury. In turn, the targeting of different purinergic receptor populations leads to a reduction in hippocampal cell death in mechanically injured organotypic slice cultures. Finally, the most promising therapeutic candidate from our *in vitro* screen (MRS 2179, a P2Y1 receptor antagonist) also improves histological and cognitive outcomes in a preclinical model of traumatic brain injury. This work shows the potential of studying astrocyte signalling after trauma to yield new and effective therapeutic targets for treating traumatic brain injury.

Keywords: neuroprotection; calcium waves; *in vivo* imaging; MRS 2179; astrocytes

Abbreviations: BAPTA-AM = 1,2-Bis(2-aminophenoxy)ethane-N,N,N′,N′-tetraacetic acid tetrakis(acetoxymethyl ester); PPADS = pyridoxalphosphate-6-azophenyl-2′,4′-disulphonic acid

Introduction

Traumatic brain injury affects nearly 10 million people worldwide each year and will become the third highest cause of death and disability in the world population by 2020 (Peden *et al*., 2004). The public awareness of traumatic brain injury is increasing, as it is known as the 'signature injury' from the Iraq and Afghanistan conflicts (Corrigan *et al*., 2010; Risdall and Menon, 2011) and

Received January 20, 2012. Revised August 3, 2012. Accepted September 3, 2012. Advance Access publication January 4, 2013

may be a risk factor for neurodegenerative disease later in life (Van Den Heuvel *et al*., 2007). Despite the clear need for treatments to improve outcome and reduce the long-term effects of traumatic brain injury, >24 clinical trials have not yielded an effective universal treatment for traumatically brain-injured patients (Maas *et al*., 2010).

Studying astrocytes, rather than neurons, after a traumatic brain injury can reveal alternative therapeutic targets. Although a key function of astroglia is to remove and recycle glutamate from the synaptic cleft (Nedergaard *et al*., 2003), studies in the past two decades have revealed that astrocytes also release neurotransmitters, such as glutamate (Parpura *et al*., 1994) and ATP (Newman, 2001). The glial release of neurotransmitters is significant because neuroglial communication influences neuronal activity (Fellin *et al*., 2004), plasticity of neuronal circuits (Gordon *et al*., 2009), as well as neuronal survival (Ding *et al*., 2007). The vesicular release of neurotransmitters, such as glutamate, is triggered by intracellular elevations in calcium (Parpura *et al*., 1994).

The intercellular propagation of calcium waves throughout the astrocyte network can be mediated by diffusion of intracellular inositol 1,4,5-trisphosphate (IP3) through gap junctions between neighbouring astrocytes (Venance *et al*., 1997), paracrine stimulation of purinergic receptors by glial release of ATP (Guthrie *et al*., 1999) or a combination of these mechanisms (Charles, 1998). Mechanical trauma stimulates calcium influx and release from intracellular stores (Rzigalinski *et al*., 1998) that triggers ATP release from astrocytes *in vitro*, which activates P2X2 and P2Y1 receptors (Neary *et al*., 2003). Indeed, mechanical stimulation of even a single astrocyte will elicit an intercellular wave among a much larger astrocyte population (Charles *et al*., 1991; Venance *et al*., 1997). Hence, these waves are a mechanism to communicate a local chemical or physical stimulus into regions well beyond the initial activation zone.

The Cornu Ammonis 3 (CA3) subregion of the hippocampus is particularly susceptible to degeneration in preclinical animal models of neurotrauma, even though this region lies deeper in the brain, beneath the epicentre of mechanical impact (Smith *et al*., 1995). The cause of preferential post-traumatic cell death in CA3 remains uncertain, but it may be attributed to differences in the mechanical compliance of CA3 (Elkin *et al*., 2007) or reduced hyperpolarization that leads to increased excitotoxicity (Deng and Xu, 2011). Interestingly, approximately half of the synapses in the hippocampal CA1 region are ensheathed by astrocytes (Ventura and Harris, 1999), thereby suggesting that mechanotransmission in astrocytes could play a prominent role in extending the penumbra of post-traumatic cell death after traumatic brain injury.

In this study, we examine the signalling initiated through the astrocyte network after neurotrauma. We target one major consequence of mechanotransmission through the astrocyte syncytium—the broad activation of purinergic signalling throughout the brain—to identify a new therapeutic direction that improves cognitive outcome and reduces neuronal loss after traumatic brain injury.

Materials and methods

Dissociated cultures

All animal procedures were approved by our institution's animal care and use committee. Primary-astrocyte cultures were isolated from Day 18 Sprague-Dawley embryos. Pregnant rats were euthanized by CO_2 inhalation followed by cervical dislocation. Embryos were removed by caesarian section, and cortices were isolated in sterile ice-cold Hank's balanced salt solution (Invitrogen) supplemented with 1 M of HEPES. Cortices were incubated in trypsin (0.3 mg/ml) and DNase I (0.2 mg/ml, Amersham Biosciences) at 37°C for 20 min. Trypsin and DNase were removed and enzymatic activity was inhibited by adding soybean trypsin inhibitor (0.5 mg/ml, Gibco). Cells were mechanically dissociated, then centrifuged for 5 min at 100*g* and resuspended in Dulbecco's modified Eagle's medium (Cambrex) with 5% foetal bovine serum (Hyclone). Cells were filtered sequentially through 60 μm and then 28 μm Nitex meshes (Cross Wire Cloth and Manufacturing Co.). Cells were plated on poly-L-lysine (Sigma) treated T75 tissue culture flasks (Fisher Scientific) at a concentration of 1×10^5 cells/ml. Cells were incubated at 37°C with 5% CO_2 and were fed twice weekly.

To develop pure astrocyte cultures, cells at 13 days *in vitro* were placed on an orbital shaker at 250 rpm overnight at 37°C, 5% CO_2 to remove the loosely adherent neuronal layer. Flasks were rinsed with saline solution before adding 4 ml of trypsin/EDTA (0.25%, Invitrogen) for 2–3 min at 37°C, and the cell layer was mechanically dislodged from the flask surface. Dulbecco's modified Eagle's medium + 5% foetal bovine serum was added to inhibit enzymatic activity. The cells were centrifuged for 5 min at 1000*g* and were resuspended in Dulbecco's modified Eagle's medium + 5% foetal bovine serum. The cell suspension was diluted to 1×10^5 cells/ml and was replated onto poly-L-lysine-treated silicone-based elastic membranes (cured Sylgard® 186:Sylgard® 184 at a 7:4 ratio, Dow Corning). Media were changed at 24 h and then at every 3–4 days until its use at 13–14 days *in vitro*, at which point the cultures had reached confluence. Cultures were >95% astrocytes as determined by immunochemistry for glial fibrillary acidic protein (astrocytes), Type-3 β-tubulin (neurons) and CNPase (oligodendrocytes) counterstained with Hoechst 33342 (20 μg/ml, Invitrogen).

To develop mixed cultures of neurons and glia, cells were directly plated after isolation onto either glass bottom dishes (MatTek Corporation, P35G-1.5-14-C) or the poly-L-lysine-treated elastomeric membranes. Cells were allowed to adhere for 24 h, and media were replaced every 4 days until testing at 14–18 days *in vitro*. At this time of testing, immunohistochemistry showed ~20% astrocytes and 80% neurons in the culture, indicated by positive staining for glial fibrillary acidic protein and neurofilament, respectively.

Organotypic hippocampal slice cultures

Brains were aseptically removed from 6- to 8-day-old CD®IGS (Sprague-Dawley) rat pups (Charles River Laboratories Inc.), transferred to ice-cold Gey's salt solution (Sigma-Aldrich) supplemented with 6.5% glucose. The hippocampus was dissected from each brain hemisphere and sectioned coronally (350-μm sections) on a McIlwain Tissue Chopper (Brinkman Instruments). The hippocampal slices were carefully separated, and 1–3 slices were plated onto elastic silicone membranes that had been pretreated overnight with poly-L-lysine

(20 μg/ml) and laminin (50 μg/ml). Cultures were kept in a humidified incubator at 37°C and 5% CO_2 on a rocker (0.5 Hz, Elmeco Engineering) for 9–10 days *in vitro*, with media changes occurring every 2–3 days.

In BAPTA-AM loaded cultures (100 μM, Molecular Probes), BAPTA-AM was loaded at room temperature for 40 min. Cultures were then rinsed twice with warm medium and incubated at 37°C and 5% CO_2 for 20 min before injury. All cultures were stretched once (see later in the text) and returned to the incubator until imaging.

Cell stretch injury

Our mechanical injury device applies a rapid (20 ms) transient deformation to a 2 × 18 mm rectangular region of the cell culture surface (Fig. 2A). Cells in the penumbra of the stretched region experience no mechanical deformation (Lusardi *et al*., 2004). Deformations of 5, 15 and 25% strain were used to simulate mild, moderate and severe injuries, respectively, below the threshold for damage to the blood–brain barrier (Shreiber *et al*., 1999). In the study of post-traumatic administration of the P2Y1 antagonist MRS 2179, organotypic hippocampal cultures were stretched on a comparable biaxial stretch-injury device (Cater *et al*., 2006).

In dissociated cultures, cell viability after stretch was determined by incubating cells in propidium iodide (5 μg/ml, Molecular Probes) and Hoechst 33342 for 15 min before fixing with 4% paraformaldehyde. In hippocampal slice cultures, cells were loaded with propidium iodide 15–20 min before injury. Slices were removed from the incubator at the designated time after injury and were imaged on a confocal microscope. Propidium iodide labelling was analysed using MetaMorph software (Universal Imaging). For each hippocampal slice, a single image was chosen for analysis at a distance of 20 μm above the Sylgard® membrane surface.

Glutamate excitotoxicity

Mixed cultures of neurons and glia were subjected to 100 μM of glutamate at 14 days *in vitro*, resulting in excitotoxic cell death as evidenced by a loss of cells labelled with the neuronal marker MAP-2.

In vitro calcium imaging

Imaging of intercellular calcium waves astrocytes was done using the ratiometric calcium dye Fura-2-AM (5 μM, Invitrogen). Cells were incubated for 50 min in the dark at room temperature, rinsed with saline and incubated for an additional 10 min. Cells were imaged on a TE300 inverted microscope equipped with our cell stretching device. Fura-2 was excited with a 340 and 380 nm filter wheel, and images were acquired every 3 s with a Hamamatsu Orca ERG camera using MetaFluor imaging software (Molecular Devices). Cells were considered to be responding if the peak Fura-2 ratio after stretch was 50% higher than the mean baseline value. Cells in the penumbra were imaged by viewing through a fused silica plate that did not interfere with either the excitation or emission spectra of the Fura-2 indicator. The distance that calcium waves propagated into the penumbra was determined by measuring the distance from the edge of the stretched region to the farthest responding cell in the field of view within 1 min after stretching.

Measurements of intracellular calcium changes in neurons, used as an indicator of electrical activity, were accomplished using the calcium-sensitive fluorescent dye Fluo-4. Thirty minutes before scheduled observation, neurons were loaded with Fluo-4-AM (Invitrogen, 1 μM) at room temperature. Immediately before imaging, neuronal cultures were rinsed in buffered saline solution (CSS; 126 mM NaCl, 5.4 mM KCl, 1 mM $MgCl_2$, 1.8 mM $CaCl_2$, 10 mM HEPES, 25 mM glucose, pH 7.4) and were placed on a Nikon TE2000-U microscope, equipped with a Yokogawa spinning disk confocal unit (CSU-10B, Solamere Technologies), Coolsnap HQ2 CCD camera (Roper Scientific) and operated with MetaMorph 7.6.5.0 software (Molecular Devices). Calcium activity from 100 to 200 neurons in the field of view was recorded at 20 Hz for 5 min, using a 488-nm excitation laser (BlueSky Research, FTEC2) and Nikon × 10/0.45 Plan Apo objective. After acquiring the necessary image set, *N*-methyl-D-aspartate (100 μM) was added to the cultures to discriminate between neurons and astrocytes in the mixed culture. We confirmed the detection of different cell types in the culture using this *N*-methyl-D-aspartate stimulation method by using independent immunocytochemistry with cell-specific markers (astrocytes: glial fibrillary acidic protein; neurons: neurofilament 68kDa (NF-68)). Post-processing of images used custom-designed routines developed in MATLAB (The MathWorks Inc.) to detect peak transients for individually selected cells in the field of view, to assemble raster plots of activity in the neuronal layer and to measure changes in intracellular calcium within astrocytes of the mechanical penumbra.

Luciferin–luciferase assay

Extracellular ATP was detected using the luciferin–luciferase reaction. Astrocytes were incubated in 0.5 ml of saline containing 140 μg/ml firefly luciferase (L-1759, Sigma) and 100 μg D-luciferin sodium salt (L-6882, Sigma). Luminescence measured with a ×40 objective attached to an upright microscope equipped with a photon counting intensified charge-coupled device (CCD) camera (C2400-35). Photon counts were streamed to disk at a frequency of 30 Hz and were integrated after acquisition. Values reported are integrated counts per 3 s, normalized to the average baseline values for the 15 s before injury.

In vivo imaging calcium waves from cortical impacts

Mice (C57Bl6, Jackson) were prepared for *in vivo* imaging as previously described (Tian *et al*., 2006). Briefly, mice were anaesthetized with an intraperitoneal injection of 1.5 g/kg urethane. A 2.3-mm craniotomy was produced on the left hemisphere, midway between bregma and lambda. The dura was gently removed, being careful not to damage the underlying cortex. A head plate containing a window for the exposed cortex was cemented to the skull with Vetbond™. The exposed cortex was incubated with 0.65 mM of Fluo-4-AM (Invitrogen) diluted in 20% pluronic in dimethyl sulphoxide with artificial CSF for 1.5 h. Fluo-4 was rinsed with artificial CSF and was incubated for an additional 30 min to allow for de-esterification. The cortex was coverslipped, and 1.5% low temperature agarose was injected between the coverslip and the cortex to minimize motion artefact during *in vivo* imaging. The cortex was continuously irrigated with artificial CSF to prevent drying. This loading protocol preferentially labels astrocytes with Fluo-4 up to a depth of ~150 μm beneath the surface of the cortex (Tian *et al*., 2006). Mice were mounted in an

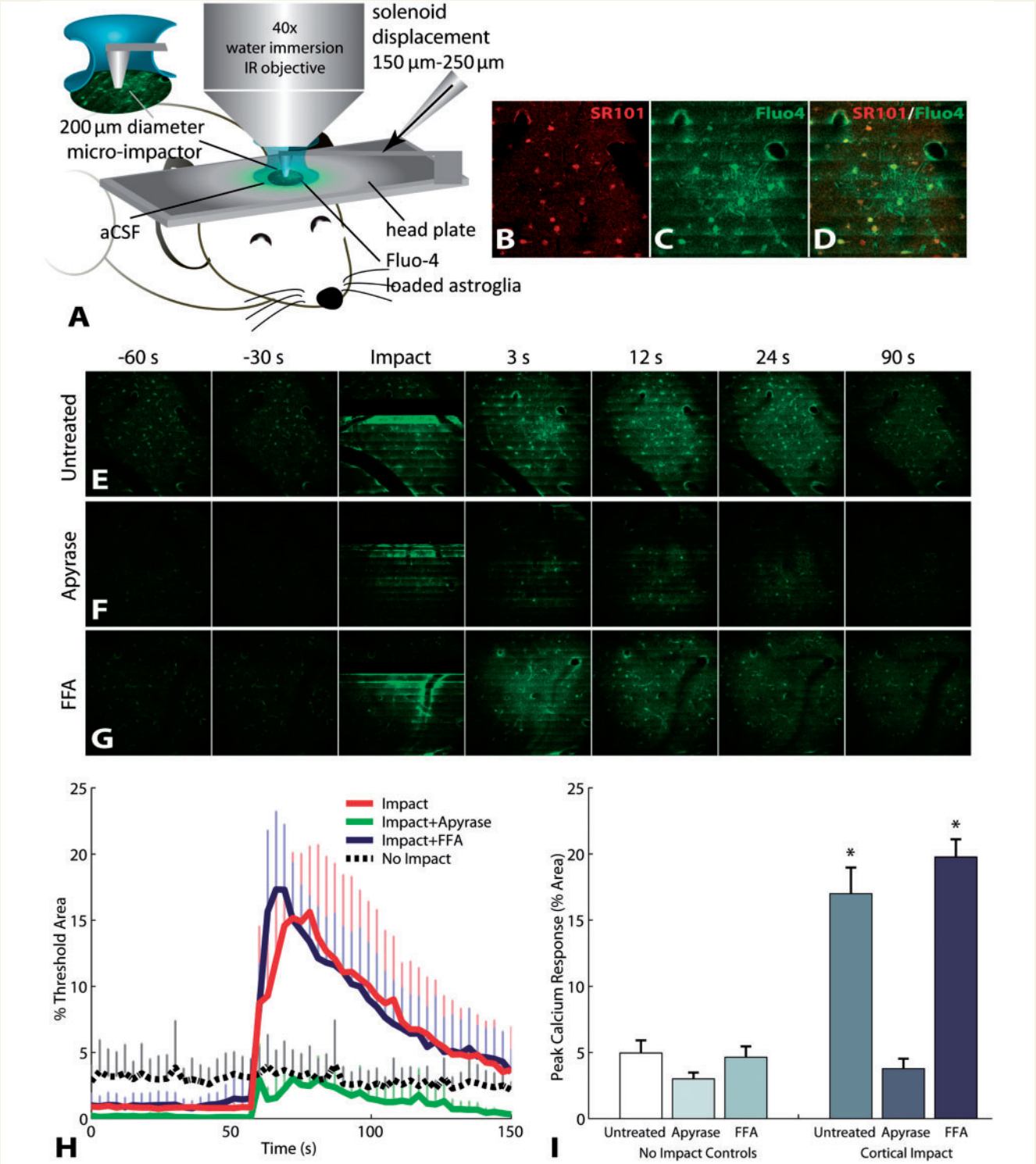

Figure 1 Mechanical impact to mouse cortex triggers astrocyte calcium waves *in vivo* that are mediated by purinergic signalling. (**A**) Calcium activity in cortical astrocytes detected by two-photon *in vivo* imaging of Fluo-4 calcium indicator. Selective loading of Fluo-4 with the astrocyte specific indicator SR101 (**B–D**). Mechanical impact triggered calcium waves in astroglia (**E** and **H**). The extent of post-traumatic calcium waves, measured by the per cent area of increased Fluo-4 fluorescence, was attenuated by degrading ATP with apyrase (**F**, **H** and **I**), but was not changed by blocking gap junctions (**G**, **H** and **I**). Error bars denote standard error of the mean (SEM) from three (non-impact) to five (impact) animals per group. FFA = flufenamic acid.

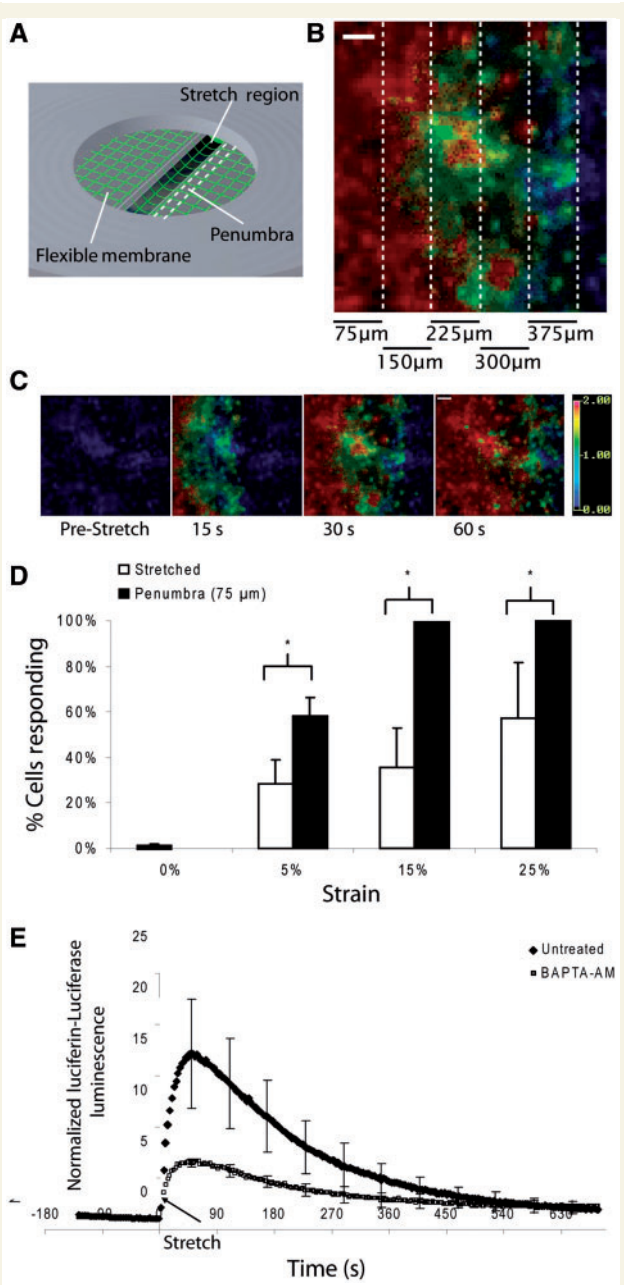

Figure 2 Mechanical stretch triggers intercellular calcium waves and ATP release in astrocytes *in vitro*. (**A**) Schematic of stretch chamber where astrocytes grown on silicone elastic membranes (green grid) were stretched by a pulse of air pressure that deflects the membrane (2×18 mm^2) through a slit in the chamber's base. The mechanical penumbra is the region adjacent to the stretched region. (**B**) Fura-2-AM imaging revealed mechanically induced intercellular calcium waves propagate from the injury epicentre outward (**C**). Colorimetric scale bar represents Fura-2 ratio (340/380 nm). (**D**) A significantly greater proportion of astrocytes in the penumbra showed increases in intracellular calcium (>50% above baseline) than astrocytes directly in the stretched region ($P < 0.05$). (**E**) Imaging of luciferin–luciferase showed mechanical stretching induced ATP release within the first minute. This increase in intracellular calcium was significantly attenuated by BAPTA-AM, indicating that the ATP release was mediated by intracellular calcium. Error bars denote SEM from 4 to 33 stretch injuries per group. Scale bars = 50 μm.

in vivo two-photon imaging system (Prairie Technologies), and images were acquired at 3 s intervals using a ×40 water-immersion infra-red objective with 820 nm excitation wavelength. Cortical impacts (200 μm) were delivered using a custom-built impactor, with a tip diameter of 200 μm (Fig. 1A).

Drug infusions and controlled cortical impact brain injuries

Eighty mice (C57Bl6, Jackson) were used for the *in vivo* study on treating brain injury with the purinergic antagonist MRS 2179 or artificial CSF vehicle control. The mice were divided into the following groups with the euthanasia time-point in days indicated in parentheses: eight naïve, 11 artificial CSF infusion control mice ($n = 5$ Day 3, $n = 6$ Day 7), 10 MRS 2179 infusion control mice ($n = 4$ Day 3, $n = 6$ Day 7), 24 injured and treated with artificial CSF infusion ($n = 11$ Day 3, $n = 13$ Day 7) and 27 injured and treated with MRS 2179 ($n = 12$ Day 3, $n = 15$ Day 7). Three days before controlled cortical impact brain injuries, mice were anaesthetized with 60 mg/kg sodium pentobarbital and an Alzet micro-osmotic mini-pump (DURECT Corporation) containing 1 mM of MRS 2179 or artificial CSF vehicle control was implanted into a dorsal subcutaneous pocket. The treatment solution was infused into the right ventricle through a 3.0 mm, 30 gauge cannula (Alzet Brain Infusion Kit 3, DURECT Corporation) that was stereotaxically positioned (Kopf Instruments) at 0.9 mm rostral to bregma and 0.6 mm lateral to the sagittal suture. A 0.8-mm burr (Meisinger) was used to drill an opening in the skull, and the cannula was lowered and cemented into place.

On the day of injury, mice were anaesthetized with 60 mg/kg of sodium pentobarbital and were placed in a stereotaxic frame. A 4-mm craniotomy was produced on the left hemisphere, midway between bregma and lambda. Moderate controlled cortical impact brain injuries were produced with a pneumatic impactor at a speed of 2.4 m/s to a cortical impact depth of 1.1 mm. The cranial exposure was sutured close, and the animals were placed in a warmed cage to recover from anaesthesia.

Morris water maze

At 3 or 7 days post-injury, the spatial learning of the mice was tested in the Morris water maze (Smith *et al*., 1995). In this test, the mice swim in opaque water searching for an escape platform. Visual cues on the walls of the water maze enable the mice to learn the position of the escape platform over eight repeated trials. The mean escape latency for the last four trials was used as a measure of the learning ability of the mouse.

Euthanasia and histology

Mice were anaesthetized with an overdose of sodium pentobarbital. Animals were transcardially perfused with 20 ml of ice-cold phosphate buffered saline (PBS) (pH 7.4) and then 40 ml of freshly hydrolysed ice-cold 4% paraformaldehyde. Brains were harvested, post-fixed overnight in 4% paraformaldehyde at 4°C and then cryoprotected in 24% sucrose. Tissue was mounted in Tissue-Tek® and was frozen in isopentane cooled with dry ice. Tissue was cryosectioned at 20 μm. Exhaustive sections were evenly distributed over five replicate series, with a spacing of 200 μm between sections within a series.

Histological sections were imaged on a Leica DM4000 microscope. Lesion volumes were calculated using Cavaleri's method (Howard and Reed, 1998) from 10 sections stained with haematoxylin and eosin.

Stereology in CA3

Cell loss in the CA3 subregion of the hippocampus was revealed by Cresyl violet staining and was quantified using stereology with optical disectors (Howard and Reed, 1998) similar to methods previously described (Baldwin *et al*., 1997; Oliveira-da-Silva *et al*., 2010). The optical disector enables total cell counts in a 3D volume to be estimated from pairs of images. Images were acquired using a $\times 40$ 0.85 numerical aperture (NA) objective lens with a Leica DFC500 camera equipped with pixel shifting technology that triples the acquired image resolution. The resultant lateral resolution was 0.1 μm per pixel with a depth of field of 0.36 μm. The microscope's *z*-position was tracked with a Heidenhain 0.05-μm-resolution length gauge (MT 1271, Heidenhain) that enabled determination of the total tissue section thickness as well as positioning the 3-μm optical disector within the middle of the tissue section. Disector images were acquired from serial sections registered to bregma, −1.4, −1.6, −1.8, −2.0 and −2.2 (Franklin and Paxinos, 1996). The CA3 subregion was manually traced, and $30 \times 30\,\mu m^2$ unbiased stereological counting frames on a $60 \times 60\,\mu m^2$ grid were randomly placed on CA3 (Fig. 6A). Standard stereology counting procedures for the optical disector were used (Howard and Reed, 1998). Nucleoli—identified by dense Nissl staining—were enumerated if they appeared within the counting frame of the reference section (Fig. 6B) and were absent from the look-up section. Nucleoli that appeared in both the reference and look-up sections (Fig. 6B and C) were not counted, nor were nucleoli that touched the forbidden lines of the counting frame (Fig. 6B). The number of cells enumerated within the counting frames was scaled by the area fraction sampled by the grid of frames and then scaled again by the volume fraction (disector thickness/tissue section thickness) to determine the total number of cells in the 3D volume. Section selection and quantitative analysis were conducted blind with counts performed on side-by-side disector counting frames rendered in custom software written in MATLAB.

Animals were excluded if a complete set of serial sections was not available at the prescribed coronal coordinates (because of imperfect cryosectioning), which resulted in the following group sizes for the stereological analysis: six naïve, eight artificial CSF infusion control mice, nine MRS 2179 infusion control mice, 17 injured and treated with artificial CSF infusion and 21 injured and treated with MRS 2179.

Statistical analysis

Data are reported as mean ± standard error and analysed by ANOVA followed by *post hoc* analysis using Student Newman-Keuls or Tukey's Honestly significant difference test for unequal group numbers. Fura-2 data were transformed using a log transform to establish homogeneity of variance. For stereological analysis, the baseline effect of cannula implantation was determined by comparing pump infusion control mice with naïve animals using one-way ANOVA (naïve, artificial CSF and MRS 2179) in each hemisphere. Infusion control mice were also analysed with two-way (time and treatment) repeated-measures ANOVA to assess the effect of artificial CSF and MRS 2179 on the contralateral side versus the uninjured lesion side. The efficacy of treating controlled cortical impact injuries with artificial CSF and MRS 2179 was analysed with three-way ANOVA (time: Day 3, Day 7; injury: pump infusion control mice, controlled cortical impact; treatment: artificial CSF, MRS 2179) in the penumbra region and the region adjacent to the lesion in both hemispheres. There was consistently no effect of time post-injury. As such, the data were pooled across days. Data were considered significant at $P < 0.05$.

Results

Mechanotransmission through the astrocyte network is mediated by purinergic signalling

We first measured the immediate response of *in vivo* astrocytes to neurotrauma, hypothesizing that mechanical injury initiates astrocyte signalling into regions distant from the initial impact site. We focused on the immediate changes in cytosolic calcium within individual astrocytes, given the role of calcium signalling in astroglial release of neurotransmitters (Haydon and Carmignoto, 2006). Micromechanical impact, or 'microTBI', of the exposed cortex to a depth of 150–200 μm clearly triggered intercellular calcium waves in cortical astrocytes (Fig. 1A–E). The addition of apyrase to degrade ATP significantly attenuated the intercellular wave appearing after microTBI (Fig. 1F, H and I). In contrast, the addition of flufenamic acid to block gap junctions did not attenuate mechanically triggered calcium waves (Fig. 1G–I). These results illustrate that mechanical trauma to astrocytes *in vivo* triggers ATP-mediated calcium waves, which transmit the impact outward, beyond the initial epicentre of mechanical trauma.

After learning that astrocyte intercellular waves after *in vivo* microTBI were mediated by ATP, we used an *in vitro* model of neurotrauma (Fig. 2A–C) to compare graded severities of trauma, to detect the release of ATP in response to calcium waves (Newman, 2001) and to identify the prominent mechanisms regulating the propagation of intercellular calcium waves. Across a spectrum of mechanical injury levels, a calcium wave proportional to the magnitude of stretch-injury propagated outward into the penumbra of the mechanical injury epicentre (Fig. 2D). Remarkably, the calcium transient caused by stretch was enhanced in the mechanical penumbra compared with the zone of primary-mechanical injury, with a significantly higher fraction of astrocytes responding in the penumbra after 15 and 25% stretch injury levels (Fig. 2D). Coincident with the progression of this intercellular wave through the astrocytes, we measured the release of ATP into the mechanical penumbra by using a luciferin–luciferase assay. Extracellular ATP levels increased over the course of 1 min after injury before recovering to baseline during the subsequent 10 min (Fig. 2E). Pretreatment of the cells with BAPTA-AM (100 μM) to chelate intracellular calcium prevented the propagation of the calcium waves into the penumbra of the stretched region and reduced the release of ATP into the extracellular environment (Fig. 2E).

We examined the relative role of mechanisms that mediate the propagation of intercellular waves through astrocytes after mechanical injury. At the lowest injury level tested (5% peak stretch), broad spectrum antagonism of P2 purinergic receptors with suramin (100 μM), pyridoxalphosphate-6-azophenyl-2′,4′-disulphonic acid (10 μM PPADS) or degradation of extracellular ATP with the enzyme apyrase (20 U/ml) attenuated the propagation of calcium waves both adjacent (75 μm) to and remote (375 μm) from the area of mechanical injury (Fig. 3A–C). At moderate injury levels (15% strain), it was necessary to block gap junctions with

flufenamic acid (30 μM) in addition to P2 purinergic signalling (10 μM of PPADS) to abolish calcium wave propagation (Fig. 3D and E; $P < 0.001$ total calcium response in presence of flufenamic acid + PPADS compared with untreated stretch injuries). At the highest level of stretch tested (25%), antagonism of P2 receptors continued to attenuate the majority of the calcium wave propagation to the remote region (Fig. 3F and G), but a cocktail of purinergic antagonists, gap junction blockers and antagonists to metabotropic glutamate receptors [100 μM of LY367385 mGluR1 antagonist and 50 μM of 2-methyl-6-(phenylethynyl)-pyridine mGluR5 antagonist] was necessary to block the signalling entirely.

Astrocyte calcium waves in the penumbra can influence the activity of injured neuronal networks

We next tested whether intercellular calcium waves within astrocytes of the mechanical penumbra influence the activity of neuronal networks. In uninjured mixed neuronal-glial cultures, functional multi-neuronal calcium imaging (Yuste *et al*., 1992; Christie *et al*., 1995; Jayaraman and Laurent, 2007) revealed spontaneous activity among neuron clusters (Fig. 4A–E), an activity pattern we confirmed with neuronal-glial cultures grown on microelectrode arrays (Supplementary Fig. 1). After mechanical injury, astrocyte intercellular calcium waves appeared in the mechanical penumbra (Fig. 4F), and both the spontaneous synchronous frequency and degree of synchronization decreased significantly in the mechanical penumbra with the onset of the intercellular wave ($P < 0.01$; Fig. 4G versus Fig. 4H, L and M). Similar to pure astrocyte cultures, mixed cultures pretreated with either BAPTA-AM, PPADS or apyrase blocked the calcium wave from appearing in astrocytes within the mechanical penumbra (Fig. 4I) and maintained post-traumatic neuronal activity at a level similar to pre-injury values (Fig. 4J versus Fig. 4K, L and M; for both metrics: $P > 0.2$ when treated with BAPTA-AM; $P > 0.1$ when treated with PPADS + apyrase).

Astrocyte calcium signalling and purinergic receptor activation contribute to cell death in the hippocampal CA3 subregion after traumatic injury

With this conspicuous role of astrocytes in mechanotransmission after trauma *in vivo* as well as *in vitro*, we sought to determine whether these calcium waves and their influence on neuronal activity ultimately mediated post-traumatic neuronal survival. Intracellular calcium waves can trigger the release of gliotransmitters (Parpura *et al*., 1994), and these gliotransmitters can stimulate neuronal *N*-methyl-D-aspartate receptors (Fellin *et al*., 2004), purinergic receptors on neurons (Pascual *et al*., 2005), and contribute to the cell death and dysfunction after injury. Mechanical injury to cultured organotypic hippocampal slices (Supplementary Fig. 2) produced a significant and selective increase in cell death within the CA3 subregion of the slice culture ($P < 0.001$; compared with

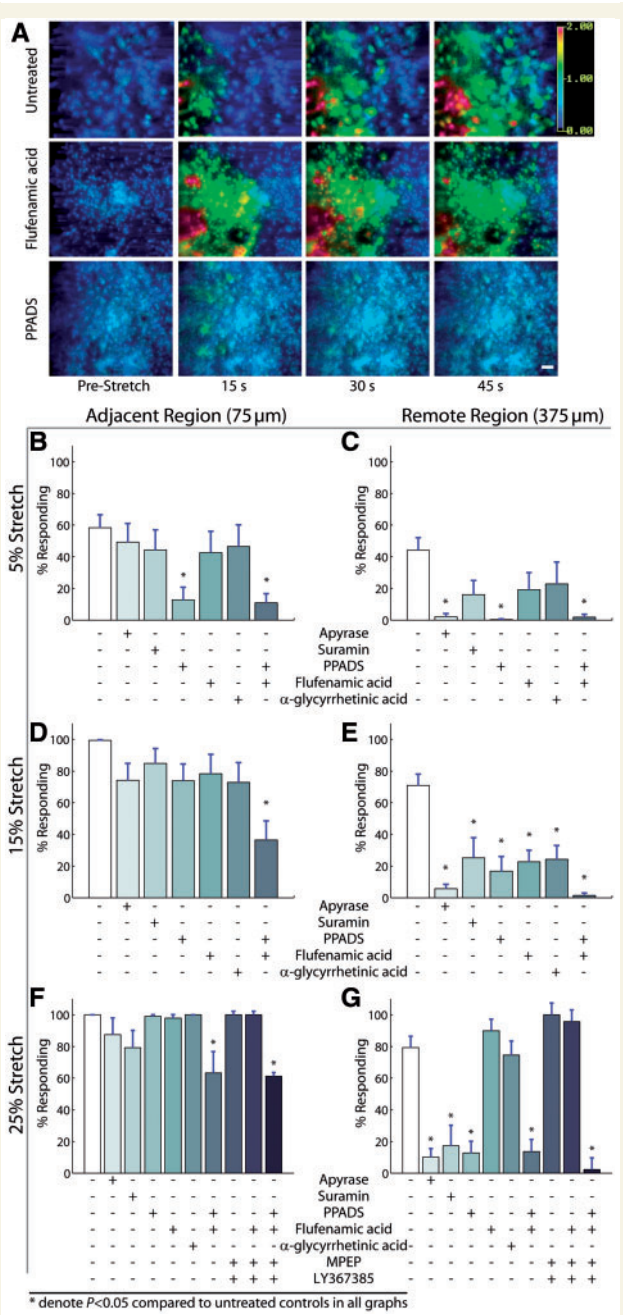

Figure 3 Purinergic signalling is a consistent mechanism of calcium-wave propagation at different injury severities. At the mildest level of mechanical trauma (5% peak stretch), propagation of calcium waves into the penumbra (**A**) was arrested from reaching the remote region (375 μm) by ATP degradation with apyrase or purinergic antagonism with PPADS but not by gap junction blockade (flufenamic acid and α-glycyrrhetinic acid) (**A–C**). At a more severe stretch (15% peak), P2 antagonism attenuated calcium waves in distant regions of the culture (375 μm from injury), and the combined inhibition of gap junctions with P2 receptors nearly abolished calcium waves in this remote region (**D** and **E**). At our most severe level of mechanical injury (25% peak stretch), purinergic antagonism reduced calcium waves in a region remote from the mechanically injured astrocytes (**F** and **G**), and a combined inhibition of purinergic receptors, gap junctions and metabotropic glutamate receptors completely blocked a calcium transient in the remote region (**G**). Error bars denote SEM from 8 to 24 stretch injuries per group.

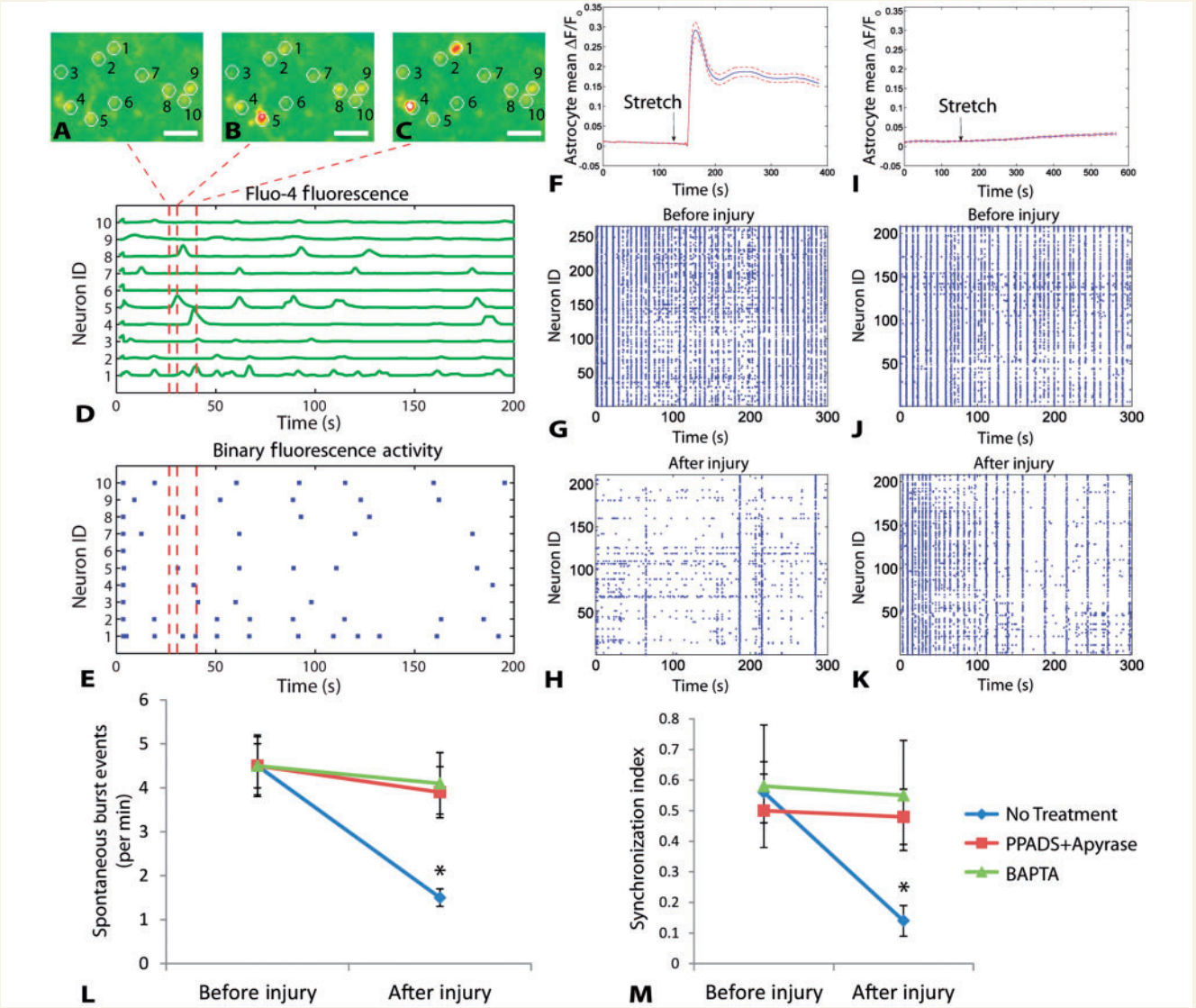

Figure 4 The activity of *in vitro* neuronal networks in the mechanical penumbra is influenced by intercellular waves in astrocytes and purinergic signalling. Mixed cultures of neurons and glia exhibited calcium oscillations detected with Fluo-4 imaging (**A–C**). (**D**) Normalized fluorescence traces show spontaneous calcium activity in the neurons numbered in **A–C**. (**E**) Fluorescence peaks (red lines in **D**) are converted into a binary raster to analyse network activity. Calcium oscillations correspond to electrical activity (Supplementary Fig. 1). Mechanical injury triggered a calcium transient in astrocytes of the mechanical penumbra within 30 s of injury (**F**). Spontaneous activity in neurons located in the mechanical penumbra decreased after injury (**G** before injury versus **H**–recording period beginning 80 s after injury when calcium wave has passed through). Pretreating mixed cultures with BAPTA-AM or a combination of PPADS and apyrase blocked the calcium wave from propagating into the mechanical penumbra (**I**) and reduced post-traumatic changes in neural activity patterns (**J** versus **K**). Both spontaneous burst events and the synchronized activity were decreased in the penumbra after injury, and these changes were blocked with PPADS + apyrase or BAPTA-AM treatment (**L** and **M**). Scale bars: **A–C** = 25 μm. Error bars in **L** and **M** = SEM from $n = 4$/group.

uninjured control cultures), as indicated by propidium iodide uptake at 24 h after injury (Fig. 5A). The increase in cell death after injury was significantly reduced by chelating calcium within astrocytes using a protocol (Liu *et al*., 2004) to preferentially load BAPTA-AM into astrocytes (Fig. 5B; selective loading shown in Supplementary Fig. 3). Elevations in intracellular calcium within astrocytes could trigger release of glutamate and activate extrasynaptic *N*-methyl-D-aspartate receptors on neurons, leading to cell death (Hardingham *et al*., 2002). In support of this possible mechanism, broad spectrum blockade of *N*-methyl-D-aspartate receptors with D-2-Amino-5-phosphonopentanoic acid (50 μM APV) significantly reduced cell death in CA3 after mechanical injury ($P < 0.05$ compared with untreated injuries; Fig. 5B).

Given the poor clinical success with *N*-methyl-D-aspartate receptor antagonists for treating traumatic brain injury (Ikonomidou and Turski, 2002), we focused on an alternative therapeutic pathway

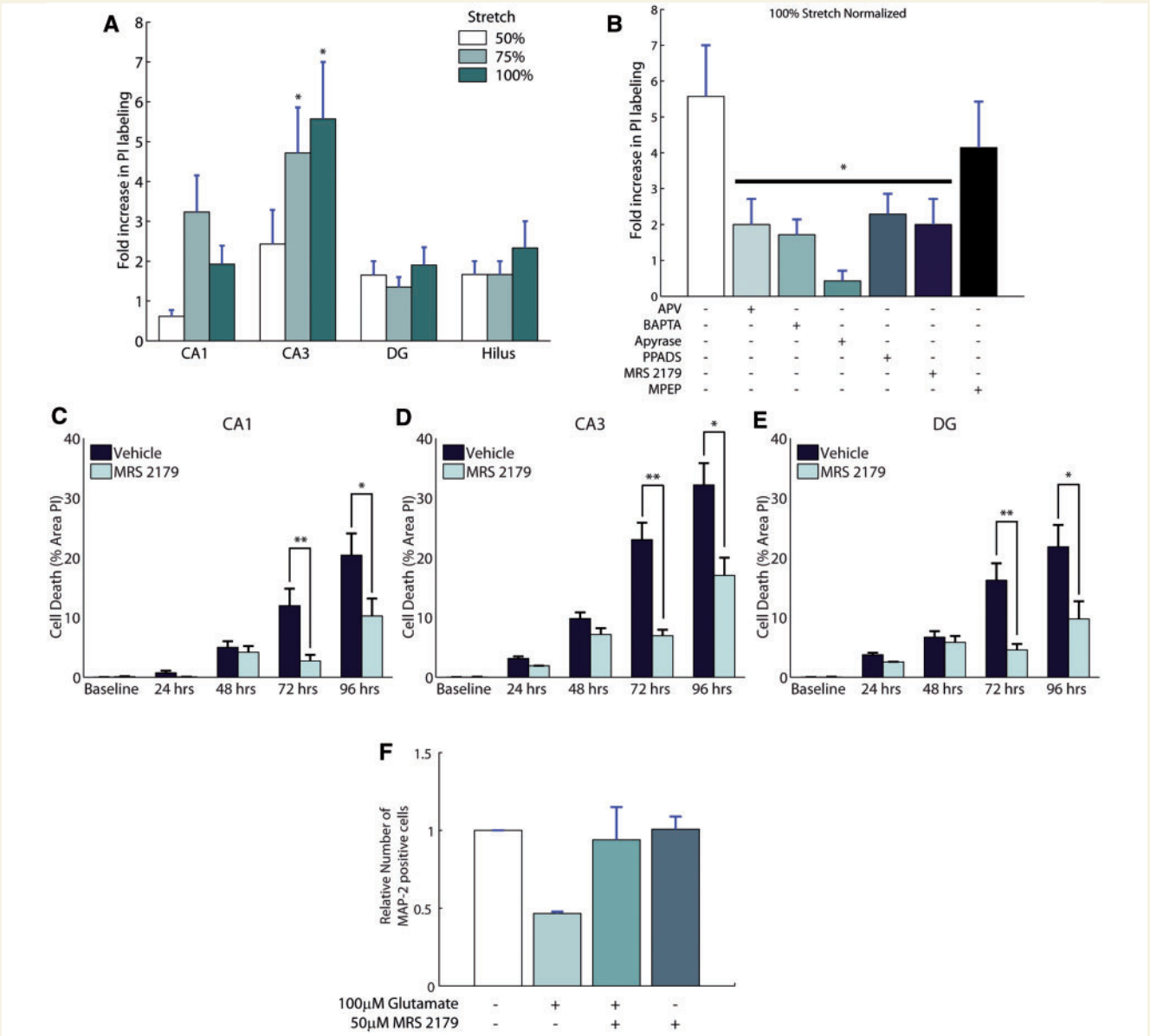

Figure 5 Purinergic antagonism is neuroprotective in stretch-injured hippocampal slices and excitotoxic insult. Organotypic slice cultures of the hippocampus were mechanically injured and evaluated for cell death using propidium iodide (PI) labelling 24 h after injury. Cell death was significantly increased in the CA3 subregion at the higher levels of mechanical injury (**A**; $n = 21–28$/group). Blocking astrocyte calcium signalling with BAPTA-AM reduced cell death in CA3, as did the broad-spectrum *N*-Methyl-D-aspartate receptor antagonist, (2R)-amino-5-phosphonovaleric acid (APV) (**B**; $n = 7–22$/group). The role of ATP in mediating the cell death after mechanical injury was significant, as apyrase treatment reduced cell death to a level similar to uninjured cultures. Antagonism of P2 receptors with PPADS, and specific antagonism of P2Y1 receptors with MRS 2179 showed equal efficacy in protecting against cell death in CA3 when applied before stretch-injury (**B**). Administration of MRS 2179 (30 μM) immediately after stretch to organotypic hippocampal slices (vehicle group 7.5 ± 3.6% stretch, $n = 40$; treated group 11.8 ± 4.6%, $n = 44$) was also neuroprotective (**C–E**). Application of 100 μM glutamate to mixed cultures of neurons and glia at 14 days *in vitro* results in excitotoxic cell death as evidenced by a loss of cells labelled with the neuronal marker MAP-2 (**F**; $n = 3$/group). Application of 50 μM MRS 2179 after glutamate stimulation protects neurons from excitotoxic cell death at 24 h. Data are presented as mean ± SEM. DG = dentate gyrus.

suggested by our collective data, that is, targeting the purinergic receptor population that could be activated in both astrocyte and neuronal networks. In untreated cultures, injury increased the level of propidium iodide labelling in CA3 by 5.6- ± 1.4-fold relative to uninjured organotypic hippocampal slices (Fig. 5B). Digesting extracellular ATP with apyrase significantly reduced propidium iodide labelling ($P < 0.05$ versus untreated cultures; $n = 7$) to 0.4- ± 0.3-fold relative to apyrase treatment without injury. The neuroprotective action of apyrase, however, is not specific, as the breakdown of ATP into the inhibitory transmitter adenosine may

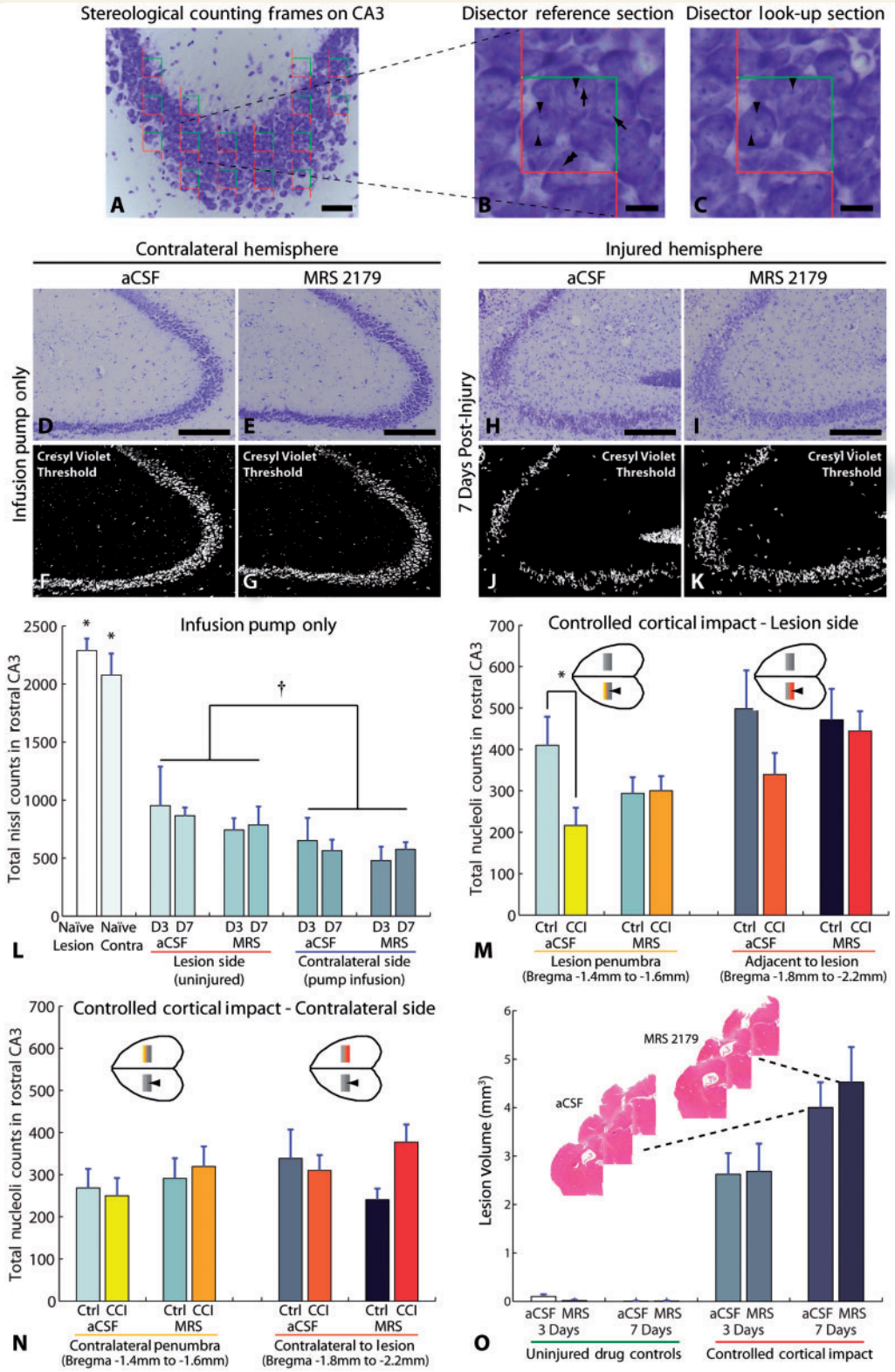

Figure 6 Antagonism of P2Y1 receptors improves hippocampal sparing after controlled cortical impact brain injury. Stereological unbiased counting frames ($30 \times 30\,\mu m^2$) arranged in a grid pattern ($60 \times 60\,\mu m^2$) were randomly overlaid on the CA3 subregion of the hippocampus to count nucleoli stained with Cresyl violet (**A**; scale bar = 50 μm). The optical disector method (**B** and **C**; disector separation = 3 μm, scale bars = 10 μm) was used to determine the number of nucleoli (dense Nissl staining) in 3D. With unbiased counting frames, the objects of interest may touch the green acceptance lines (**B** and **C**) but are not counted if they touch the red forbidden lines (double arrowhead in **B**). Additionally, in the disector method, nucleoli are counted if they lay within the counting frame of the reference section (arrows **B**) without appearing in the look-up section (**C**). Nucleoli appearing in both optical sections (arrowheads **B** and **C**) are not

(continued)

also provide neuroprotection by reducing excitatory release of synaptic glutamate through adenosine receptors (de Mendonca *et al*., 2000). A more specific treatment with PPADS (10 μM, Sigma-Aldrich), a non-selective P2 receptor antagonist with no effect on adenosine receptors, significantly reduced cell death after mechanical injury at 24 h (Fig. 5B; $P < 0.01$; $n = 24$).

To determine a more specific mechanism of neuroprotection, we antagonized the metabotropic P2Y1 receptor, known to trigger astrocytic glutamate release (Domercq *et al*., 2006), stimulate proliferation and gliotic responses (Franke *et al*., 2001) and increase inhibitory network tone among hippocampal neurons (Bowser and Khakh, 2004). Pretreatment of slice cultures with the specific P2Y1 receptor antagonist MRS 2179 (10 μM; $n = 12$) significantly reduced cell death in CA3 as evidenced by propidium iodide labelling of only 2.0- ± 0.7-fold compared with the 5.6-fold increase observed in untreated slice cultures ($P < 0.05$; Fig. 5B). Importantly, the reduction in cell death that was achieved with MRS 2179 was similar to that achieved with broad-spectrum *N*-methyl-D-aspartate receptor antagonist and broad-spectrum P2 receptor antagonist (Fig. 5B).

The effect of P2Y1 on neuroprotection was sustained, showing a significant reduction in cell death up to 96 h when treatment was applied after hippocampal injury (Fig. 5C and D). Finally, MRS 2179 treatment also protected against glutamate-induced toxicity in mixed cultures of neurons and glia, suggesting that this approach could be an effective strategy to protect against both the mechanical and neurochemical sequelae encountered in traumatic brain injury (Fig. 5F). Hence, these data indicate that in the CA3 subregion of the hippocampus, P2Y1 receptors represent a viable therapeutic target to reduce post-traumatic cell death after mechanical injury and glutamate toxicity *in vitro*.

Antagonism of P2Y1 receptors with MRS 2179 reduces loss of hippocampal neurons in the lesion penumbra and reduces cognitive deficits after controlled cortical impact brain injury in mice

With a specific purinergic receptor target established, we tested whether blockade of purinergic receptors during mechanical trauma *in vivo* could be neuroprotective. We used the controlled cortical impact model of traumatic brain injury and implanted micro-osmotic pumps into mice to deliver the P2Y1 antagonist MRS 2179 (1 mM) or artificial CSF vehicle control into the lateral ventricle 3 days before traumatic brain injury. We focused specifically on the CA3 subregion of the hippocampus, which we previously analysed in hippocampal slices, because this region is particularly susceptible to cell death after traumatic brain injury (Smith *et al*., 1995).

Qualitatively, the CA3 pyramidal cell layer appeared grossly intact in control animals that received implantation of the micro-osmotic pump and cannula without controlled cortical impact (Fig. 6D–G). In stark contrast, controlled cortical impact resulted in visible loss of CA3 pyramidal cells in the injured hemisphere (Fig. 6H–K).

Quantitatively, stereological counts of Cresyl violet-stained nucleoli revealed that control animals that received pump implantation alone exhibited a statistically significant reduction in CA3 nucleoli counts compared with naïve animals (Fig. 6L; $P < 0.001$, naïve versus artificial CSF and naïve versus MRS 2129 in all *post hoc* comparisons in both the uninjured lesion

Figure 6 Continued
counted. An estimate of the total counts in the volume is determined by scaling the counts made within the counting frames by the area fraction covered by these frames and the volume fraction sampled by the optical disector (disector thickness/measured tissue thickness). Implantation of the intraventricular cannula to deliver artificial CSF (aCSF) or MRS 2179 produced some loss in Cresyl violet staining for neurons in the CA3 pyramidal layer of uninjured animals, although CA3 appeared grossly intact (**D** and **E**; scale bars = 200 μm). Colour threshold images in **F** and **G** qualitatively illustrate slight loss of Cresyl violet staining between artificial CSF and MRS 2179 treated animals at 7 days because of the infusion alone without cortical impact. After controlled cortical impact (CCI), the CA3 subregion exhibits widespread loss of Cresyl violet staining (**H** and **I**; scale bars = 200 μm), further illustrated by colour threshold (**J** and **K**). In uninjured animals (artificial CSF $n = 4$ Day 3, $n = 4$ Day 7; MRS 2179 $n = 4$ Day 3, $n = 5$ Day 7), implantation of the cannula to infuse artificial CSF or MRS 2179 significantly reduced stereological counts of Cresyl violet-stained nucleoli in CA3 compared with completely untreated naïve control mice ($n = 6$ naïve, $^{*}P < 0.001$ for all *post hoc* comparisons between naïve and the corresponding region in infusion pump control mice). Overall, the contralateral hemisphere where the cannula was implanted exhibited a greater loss in nucleoli counts compared with the uninjured lesion side ($^{\dagger}P = 0.004$). In these infusion control mice, there was no significant difference between days ($P = 0.951$) or infusion with artificial CSF versus MRS 2179 ($P = 0.441$). After controlled cortical impact, animals treated with artificial CSF ($n = 17$) exhibited a significant reduction in counts compared with artificial CSF infusion control mice in the lesion penumbra between bregma −1.4 and −1.6 mm (**M**; $^{*}P = 0.033$). In contrast, in animals treated with MRS 2179 ($n = 21$), no additional nucleoli loss was observed in the penumbra ($P = 0.929$ MRS 2179 infusion control mice versus controlled cortical impact treated with MRS 2179, **M**). In the contralateral hemisphere, there was no statistically significant difference overall between groups (**N**). Note that counts are comparable within a given region in **M** and **N**, but the penumbra and region adjacent or contralateral to the lesion are not comparable with each other because the volume of tissue sampled and the geometry of the hippocampus are both different. Insets in **M** and **N** highlight regions shown on bar graphs along with the controlled cortical impact epicentre denoted by arrowheads (illustration is not to scale). (**O**) Lesion volumes in the cortex were not significantly different between animals treated with MRS 2179 and those treated with artificial CSF vehicle control. Lesion = lesion side in controlled cortical impact mice; Contra = contralateral side to controlled cortical impact lesion; Ctrl = pump infusion control mice without injury. Data are presented as mean ± SEM.

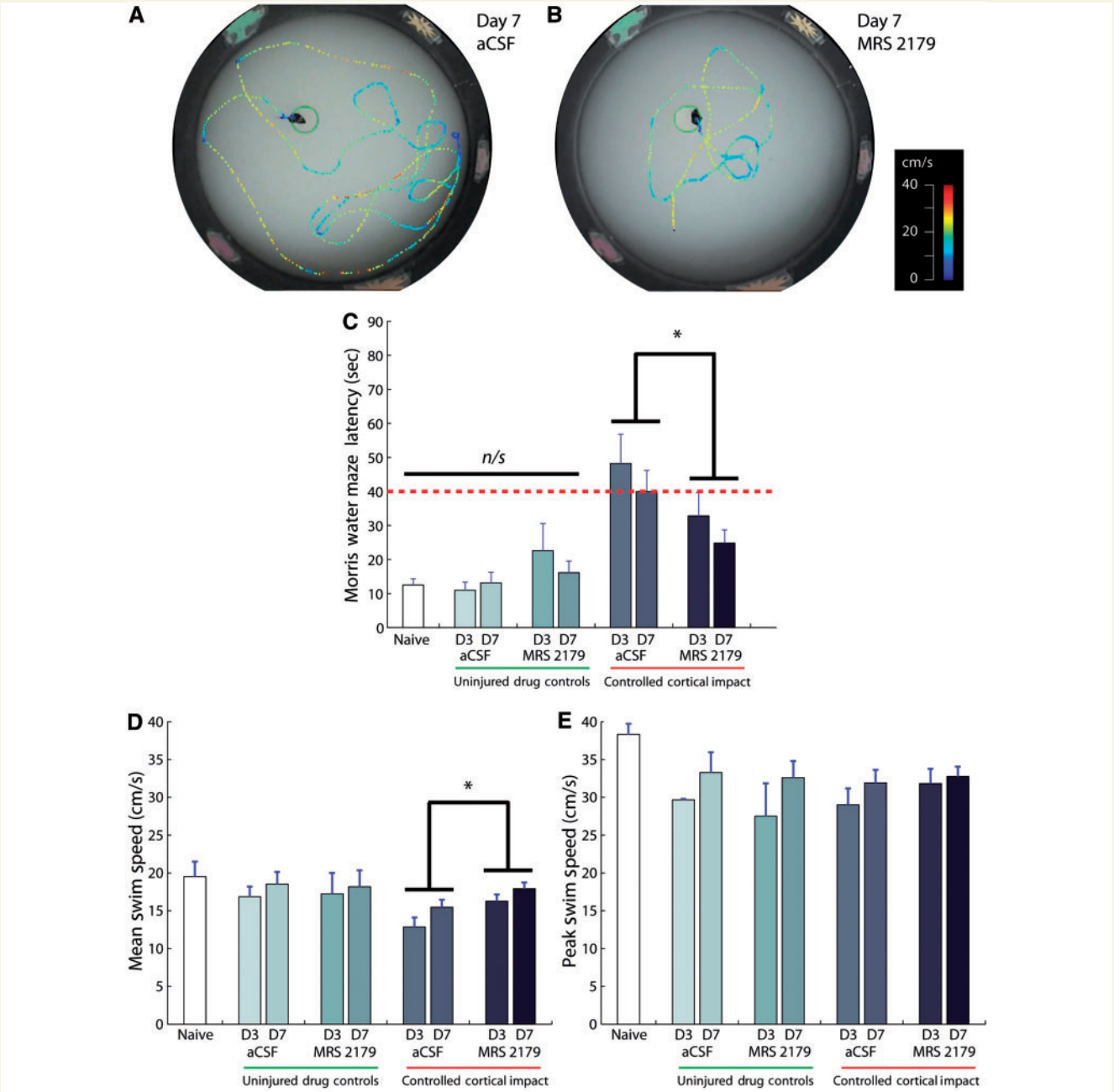

Figure 7 Antagonism of P2Y1 receptors reduced post-traumatic learning deficits after controlled cortical impact brain injury. Escape latency from Morris water maze indicates spatial learning ability of mice where a longer escape time is indicative of learning deficits (compare **A** and **B**; dotted contours indicate swim path, colour indicates speed). (**C**) Bar graphs show escape latency after controlled cortical impact (*$P = 0.019$). (**D**) Average swim speed showed a significant improvement with MRS 2179 treatment compared with artificial CSF (aCSF) infusion (*$P = 0.015$). (**E**) Peak swim speed was not different among treatment groups (artificial CSF, MRS 2179) at any time point after injury. Data are presented as mean ± SEM from $n = 8$ naïve; $n = 11$ artificial CSF uninjured; $n = 10$ MRS uninjured; $n = 11$ artificial CSF Day 3 controlled cortical impact; $n = 13$ artificial CSF Day 7 controlled cortical impact; $n = 12$ MRS Day 3 controlled cortical impact; $n = 15$ MRS Day 7 controlled cortical impact. D3 = Day 3; D7 = Day 7.

side and contralateral side where the cannula was implanted). In these pump infusion control mice, two-way repeated-measures (lesion and contralateral in same animal) ANOVA comparing the effects of time (Day 3, Day 7) and type of treatment infused (artificial CSF, MRS 2179) showed no overall difference between Day 3 and Day 7 ($P = 0.951$) or difference between artificial CSF infusion and MRS 2179 infusion ($P = 0.441$). The analysis detected a statistically significant reduction in overall nucleoli counts on the contralateral side where the cannula was implanted compared with the uninjured control lesion side (Fig. 6L; $P = 0.004$, overall

lesion side versus contralateral side). In summary, these control animals revealed that implantation of the osmotic mini-pump reduced CA3 nucleoli counts in both hemispheres, the hemisphere where the cannula was implanted exhibited a greater loss of nucleoli counts and the extent of this loss was similar between artificial CSF and MRS 2179 infusion.

After controlled cortical impact, we investigated whether neuroprotection differed between regions near the injury epicentre compared with more remote regions, similar to our observations on calcium wave propagation *in vitro* (Figs 2 and 3). We separated our CA3 nucleoli counts into two regions. We designated the counts from bregma −1.4 to −1.6 mm as the penumbra region, and the counts from bregma −1.8 to −2.2 mm as the region adjacent to the lesion epicentre (at bregma −2.0 mm). There was no effect of time post-injury for all regions ($P > 0.136$ at lesion and penumbra in both hemispheres), and the data were pooled across days. In the lesion penumbra, a two-way ANOVA comparing treatment (artificial CSF, MRS 2179) and injury (infusion pump control mice, controlled cortical impact) detected a statistically significant interaction between treatment and injury ($P = 0.045$). *Post hoc* comparisons showed that controlled cortical impact resulted in significant cell loss in the penumbra of artificial CSF-treated animals (Fig. 6M; $P = 0.033$, 410 ± 59 nucleoli counts in artificial CSF infusion control mice versus 216 ± 40 counts in artificial CSF-treated controlled cortical impact). In contrast, no additional cell loss was detected in the lesion penumbra of animals treated with MRS 2179 (Fig. 6M; $P = 0.929$, 294 ± 55 nucleoli counts in MRS 2179 infusion control mice versus 300 ± 36 counts in controlled cortical impact treated with MRS 2179). Adjacent to the lesion, between bregma −1.8 and −2.2 mm, a similar pattern of counts was observed; however, this interaction between treatment and injury was no longer statistically significant (Fig. 6M; $P = 0.321$).

In the contralateral hemisphere, we found no differences between artificial CSF and MRS 2179 treatment in the penumbra region ($P = 0.390$ artificial CSF versus MRS 2179; Fig. 6N). Contralateral to the lesion epicentre, there was no main effect of treatment (Fig. 6N; $P = 0.759$), although a slight trend ($P = 0.097$) in the interaction between treatment and injury reflects the observation that there were slightly fewer nucleoli counts with chronic MRS 2179 infusion compared with infusion in the presence of controlled cortical impact (Fig. 6N).

Additional histological analysis of the lesion volume in the brain showed no significant difference between animals treated with MRS 2179 and vehicle control at either 3 or 7 days post-trauma (Fig. 6O).

The neuroprotective efficacy of P2Y1 antagonism was also evident in the cognitive performance of these animals. The escape latency from the Morris water maze was used to assess the spatial learning ability of the mice (Fig. 7A and B). In uninjured control animals, infusion of artificial CSF or MRS 2179 did not produce significant learning deficits compared with naïve mice (Fig. 7C). In contrast, following injury, the escape latency from the water maze revealed that antagonism of P2Y1 receptors significantly improved post-traumatic spatial learning compared with vehicle treatment (Fig. 7C; $P = 0.019$ artificial CSF versus MRS 2179, $P = 0.204$ Day 3 versus Day 7, non-significant interaction). Subsequent analysis of swim speeds among the treatment groups showed that animals treated with MRS 2179 exhibited a higher average swim speed (Fig. 7D). The peak swim speed, however, was similar between animals treated with MRS 2179 and vehicle control (Fig. 7E), thereby suggesting overall motor impairments were similar. Hence, the improvement in escape latency and average swim speed after purinergic antagonism may be attributed to improved cognitive function.

Discussion

We studied the process of mechanotransmission in astrocytes to understand whether there were broad signals transmitted through the brain during and after trauma that could influence neuronal survival and cognitive deficits after traumatic brain injury. We found mechanical injury causes the release of ATP from astroglia and initiates widespread intercellular calcium waves through astrocytes *in vitro* as well as *in vivo*. Increases in astrocyte intracellular calcium influence neural activity in regions remote from the mechanical injury epicentre, and selectively attenuating intracellular calcium elevation within astrocytes reduces cell death in the CA3 region of organotypic slice cultures exposed to traumatic mechanical injury. The broad importance of purinergic signalling was also evident after *in vivo* traumatic brain injury, as P2Y1 purinergic receptor antagonism reduced post-traumatic cognitive deficits in mice. Together, these results show that mechanically triggered signalling through astrocytes significantly contributes to the pathobiology of traumatic brain injury. Consequently, targeting receptors on astrocytes and neurons that are activated by gliotransmitters provides a new therapeutic target for treating traumatic brain injury.

Traumatic brain injury is a complex and evolving disease, and some treatments have progressed recently to human clinical trials (Maas *et al*., 2010). Remarkably, however, few studies have targeted gliocentric mechanisms to develop new interventions for traumatic brain injury. Although our approach focuses on the events triggered in astrocytes during and after injury, we expect that the broad manipulation of purinergic signalling will affect both neuronal and glial networks in the recovering brain. Presynaptically, ATP inhibits the release of glutamate (Mendoza-Fernandez *et al*., 2000), although high doses of ATP will facilitate glutamate release through P2X receptor activation (Rodrigues *et al*., 2005). The likely rapid enzymatic breakdown of ATP into adenosine also suggests a potential role for the activation of adenosine receptors, which will inhibit presynaptic release through a reduction in presynaptic calcium currents (Wu and Saggau, 1994). Even with a more targeted inhibition of P2Y1 receptors, the improvement in functional outcome may be targeted to both neuronal and glial receptors. Inhibiting P2Y1 receptors on astrocytes can limit vesicular glutamate release from astrocytes (Domercq *et al*., 2006), reducing the activation of extrasynaptic *N*-methyl-D-aspartate receptors on neurons (Bezzi *et al*., 2004; Jourdain *et al*., 2007), and therefore, suppress signalling of a pathway commonly associated with neuronal death through the mitochondria (Hardingham *et al*., 2002; Starkov *et al*., 2004). Our data at least partly support this potential

protective mechanism, as the neuroprotection afforded by purinergic antagonism was similar to broad-spectrum *N*-methyl-D-aspartate receptor antagonism.

Purinergic (P2Y1) receptors are also found at neuronal synapses (Rodrigues *et al*., 2005; Tonazzini *et al*., 2007). Activation of P2Y1 receptors on hippocampal interneurons increases synaptic inhibition (Bowser and Khakh, 2004; Kawamura *et al*., 2004). Additionally, activation of presynaptic P2Y1 receptors will inhibit presynaptic glutamate release in hippocampal neurons (Mendoza-Fernandez *et al*., 2000). Therefore, blocking neuronal P2Y1 receptors leads to a general reduction in the inhibitory tone of the hippocampal circuitry, providing an enhancement of synaptic signalling through the excitatory networks. Neuroprotection through reduced synaptic inhibition initially seems counterintuitive. Evidence in the literature, however, suggests that modest synaptic stimulation triggers pro-survival pathways and antioxidant signalling (Hardingham and Bading, 2002, 2010). Therefore, it seems possible that the neuroprotection provided by P2Y1 antagonists has two components: the reduction in the release of glutamate from astrocytes, and the restoration of pro-survival synaptic signalling.

It remains unclear, however, what the optimal level of synaptic signalling is that supports neuronal survival without triggering deleterious excitotoxic pathways. Interestingly, we noticed a slight reduction in nucleoli counts in MRS 2179 infusion control mice compared with artificial CSF infusion control mice (Fig. 6L). Conversely, we observed a slight increase in cell counts in the contralateral hemisphere after controlled cortical impact (Fig. 6N). Although these differences were not detected as statistically significantly, we propose that by modulating the level of synaptic activity, MRS 2179 could be deleterious in a healthy brain by overstimulating synapses. In the injured brain, this enhanced activity may compensate for the lost pro-survival signalling of disrupted synaptic connections. Hence, purinergic receptor antagonists may provide different mechanisms of neuroprotection through neurons and glia, but these mechanisms seem to work together to improve outcome after traumatic mechanical injury.

We focused on the hippocampus because some of these synapses are ensheathed by glia, and consequently, we hypothesized that the interruption of glial mechanotransmission during injury might be beneficial. We cannot rule out, however, that other brain regions could be affected by purinergic antagonism. We did not observe obvious histological differences in the thalamus or striatum. In our controlled cortical impact model at a moderate severity, these areas do not exhibit the same stark loss of cells as in the CA3 pyramidal cell layer, but subtler changes, such as compensatory alterations in receptor expression, may have been present.

The neuroprotective effects of purinergic antagonism in the hippocampus did not seem to extend to the haemorrhagic lesion in the cortex. A recent study in a rat thoracic spinal cord injury model also did not find a neuroprotective effect of purinergic antagonism at the lesion epicentre (Rodriguez-Zayas *et al*., 2012). Instead, purinergic antagonism seemed to reduce the astrogliotic response that normally acts to contain lesion growth (Myer *et al*., 2006). Our data suggest that purinergic antagonism may have clearer neuroprotective effects in the penumbra of the injury (Figs 2, 3 and 6) rather than at the lesion epicentre where overt cellular disruption—exacerbated by haemorrhage—and the need for local astrogliosis may supersede any protection afforded by interrupting long-distance glial mechanotransmission. We attribute the cognitive improvements observed to hippocampal sparing. In contrast, functional improvements in thoracic spinal cord injury are dominated by sparing of ascending and descending long axonal tracts rather than rostrocaudal sparing in the grey matter (Hedel and Curt, 2006). Any neuroprotection afforded by purinergic antagonism of glial and synaptic receptors in the penumbra of the thoracic spinal cord lesion could be difficult to detect if these white matter tracts are already compromised at the lesion epicentre. It would be important in the future to determine the relevant volume of the injury penumbra, and correspondingly, which structures might be most amenable to neuroprotection by purinergic antagonism. An interesting observation from our *in vitro* studies is that purinergic antagonism may be beneficial over a broader spectrum of injury severities (Fig. 3); hence, it may be a more robust therapeutic avenue.

Pre-administration of MRS 2179 enabled us to assess the maximal effect of P2Y1 inhibition, but pre-administration of purinergic antagonist is not a clinically viable neuroprotection strategy. A consideration for future studies is the delivery method, which is complicated by the cardiovascular effects of P2Y1 antagonism if the drug is delivered systemically (Kunapuli *et al*., 2003). For this reason, we chose direct pharmacological administration through the intraventricular infusion pump. A disadvantage of our current delivery method is the thinning of the CA3 layer that occurs in vehicle-control mice, which indicates chronic implantation of the cannula has some adverse effects, and that treatment efficacy after controlled cortical impact should be interpreted relative to this baseline. Interestingly, we observed a trend in the statistical interaction between MRS 2179 infusion with and without injury contralateral to the lesion epicentre (Fig. 6N). The trend suggests that purinergic antagonism is beneficial in the presence of controlled cortical impact, whereas chronic MRS 2179 administration in uninjured tissue tends to reduce nucleoli counts. Hence, post-injury administration of MRS 2179 may have fewer side effects than the chronic antagonism modelled here. Defining the therapeutic window as well as the dosing regimen for this approach would be a key next step. A recent study found MRS 2179 reduced infarct volume when administered as late as 24 h after cerebral ischaemia (Kuboyama *et al*., 2011). Although ischaemia mechanisms differ from the astrocyte mechanotransmission, we analysed here, encouragingly, we also observed that post-injury treatment of organotypic slices with MRS 2179 blocked cell death (Fig. 5C–E), thereby raising the possibility that a P2Y1-based approach has translational utility.

The results presented here add to the complex role of astrocytes in neurotrauma. Although post-traumatic reactive astrogliosis forms a physical and biochemical barrier that inhibits axonal regeneration (Yiu and He, 2006), the early traumatic response of astroglia is thought to be neuroprotective, as astrocyte ablation worsens traumatic brain injury (Faulkner *et al*., 2004; Myer *et al*., 2006). Here, we report that during the primary-mechanical trauma, mechanotransmission through astrocytes may play a leading role in mediating neuronal fate and impairment after traumatic

brain injury. As such, this work could highlight an important therapeutic direction for improving outcome after traumatic brain injury.

Acknowledgements

The authors thank Dr M. Halassa for advice on pump implantation, as well as B. Wierzbicki and K. McManus for technical assistance.

Funding

National Institutes of Health (NS 35712, HS 41699); Department of Defense (W911NF-10-1-0526); the State of New Jersey (10-3209-BIR-E-3).

Supplementary material

Supplementary material is available at *Brain* online.

References

Baldwin SA, Gibson T, Callihan CT, Sullivan PG, Palmer E, Scheff SW. Neuronal cell loss in the CA3 subfield of the hippocampus following cortical contusion utilizing the optical disector method for cell counting. J Neurotrauma 1997; 14: 385–98.

Bezzi P, Gundersen V, Galbete JL, Seifert G, Steinhauser C, Pilati E, et al. Astrocytes contain a vesicular compartment that is competent for regulated exocytosis of glutamate. Nat Neurosci 2004; 7: 613–20.

Bowser DN, Khakh BS. ATP excites interneurons and astrocytes to increase synaptic inhibition in neuronal networks. J Neurosci 2004; 24: 8606–20.

Cater HL, Sundstrom LE, Morrison B III. Temporal development of hippocampal cell death is dependent on tissue strain but not strain rate. J Biomech 2006; 39: 2810–18.

Charles A. Intercellular calcium waves in glia. Glia 1998; 24: 39–49.

Charles AC, Merrill JE, Dirksen ER, Sanderson MJ. Intercellular signaling in glial cells—calcium waves and oscillations in response to mechanical stimulation and glutamate. Neuron 1991; 6: 983–92.

Christie BR, Eliot LS, Ito K, Miyakawa H, Johnston D. Different Ca2 + channels in soma and dendrites of hippocampal pyramidal neurons mediate spike-induced Ca2 + influx. J Neurophysiol 1995; 73: 2553–7.

Corrigan JD, Selassie AW, Orman JA. The epidemiology of traumatic brain injury. J Head Trauma Rehabil 2010; 25: 72–80.

de Mendonca A, Sebastiao AM, Ribeiro JA. Adenosine: does it have a neuroprotective role after all? Brain Res Brain Res Rev 2000; 33: 258–74.

Deng P, Xu ZC. Contribution of Ih to neuronal damage in the hippocampus after traumatic brain injury in rats. J Neurotrauma 2011; 28: 1173–83.

Ding S, Fellin T, Zhu Y, Lee SY, Auberson YP, Meaney DF, et al. Enhanced astrocytic Ca2 + signals contribute to neuronal excitotoxicity after status epilepticus. J Neurosci 2007; 27: 10674–84.

Domercq M, Brambilla L, Pilati E, Marchaland J, Volterra A, Bezzi P. P2Y1 receptor-evoked glutamate exocytosis from astrocytes: control by tumor necrosis factor-alpha and prostaglandins. J Biol Chem 2006; 281: 30684–96.

Elkin BS, Azeloglu EU, Costa KD, Morrison B III. Mechanical heterogeneity of the rat hippocampus measured by atomic force microscope indentation. J Neurotrauma 2007; 24: 812–22.

Faulkner JR, Herrmann JE, Woo MJ, Tansey KE, Doan NB, Sofroniew MV. Reactive astrocytes protect tissue and preserve function after spinal cord injury. J Neurosci 2004; 24: 2143–55.

Fellin T, Pascual O, Gobbo S, Pozzan T, Haydon PG, Carmignoto G. Neuronal synchrony mediated by astrocytic glutamate through activation of extrasynaptic NMDA receptors. Neuron 2004; 43: 729–43.

Franke H, Krugel U, Schmidt R, Grosche J, Reichenbach A, Illes P. P2 receptor-types involved in astrogliosis in vivo. Br J Pharmacol 2001; 134: 1180–9.

Franklin KBJ, Paxinos G. The mouse brain in stereotaxic coordinates. San Diego, CA: Academic Press; 1996.

Gordon GR, Iremonger KJ, Kantevari S, Ellis-Davies GC, MacVicar BA, Bains JS. Astrocyte-mediated distributed plasticity at hypothalamic glutamate synapses. Neuron 2009; 64: 391–403.

Guthrie PB, Knappenberger J, Segal M, Bennett MV, Charles AC, Kater SB. ATP released from astrocytes mediates glial calcium waves. J Neurosci 1999; 19: 520–8.

Hardingham GE, Bading H. Coupling of extrasynaptic NMDA receptors to a CREB shut-off pathway is developmentally regulated. Biochim Biophys Acta 2002; 1600: 148–53.

Hardingham GE, Bading H. Synaptic versus extrasynaptic NMDA receptor signalling: implications for neurodegenerative disorders. Nat Rev Neurosci 2010; 11: 682–96.

Hardingham GE, Fukunaga Y, Bading H. Extrasynaptic NMDARs oppose synaptic NMDARs by triggering CREB shut-off and cell death pathways. Nat Neurosci 2002; 5: 405–14.

Haydon PG, Carmignoto G. Astrocyte control of synaptic transmission and neurovascular coupling. Physiol Rev 2006; 86: 1009–31.

Hedel HJ, Curt A. Fighting for each segment: estimating the clinical value of cervical and thoracic segments in SCI. J Neurotrauma 2006; 23: 1621–31.

Howard CV, Reed MG. Unbiased stereology—three dimensional measurement in microscopy. New York: Springer; 1998.

Ikonomidou C, Turski L. Why did NMDA receptor antagonists fail clinical trials for stroke and traumatic brain injury? Lancet Neurol 2002; 1: 383–6.

Jayaraman V, Laurent G. Evaluating a genetically encoded optical sensor of neural activity using electrophysiology in intact adult fruit flies. Front Neural Circuits 2007; 1: 3.

Jourdain P, Bergersen LH, Bhaukaurally K, Bezzi P, Santello M, Domercq M, et al. Glutamate exocytosis from astrocytes controls synaptic strength. Nat Neurosci 2007; 10: 331–9.

Kawamura M, Gachet C, Inoue K, Kato F. Direct excitation of inhibitory interneurons by extracellular ATP mediated by P2Y1 receptors in the hippocampal slice. J Neurosci 2004; 24: 10835–45.

Kuboyama K, Harada H, Tozaki-Saitoh H, Tsuda M, Ushijima K, Inoue K. Astrocytic P2Y(1) receptor is involved in the regulation of cytokine/chemokine transcription and cerebral damage in a rat model of cerebral ischemia. J Cereb Blood Flow Metab 2011; 31: 1930–41.

Kunapuli SP, Ding ZR, Dorsam RT, Kim S, Murugappan S, Quinton TM. ADP receptors-targets for developing antithrombotic agents. Curr Pharm Des 2003; 9: 2303–16.

Liu QS, Xu QW, Arcuino G, Kang J, Nedergaard M. Astrocyte-mediated activation of neuronal kainate receptors. Proc Natl Acad Sci USA 2004; 101: 3172–7.

Lusardi TA, Rangan J, Sun D, Smith DH, Meaney DF. A device to study the initiation and propagation of calcium transients in cultured neurons after mechanical stretch. Ann Biomed Eng 2004; 32: 1546–58.

Maas AI, Roozenbeek B, Manley GT. Clinical trials in traumatic brain injury: past experience and current developments. Neurotherapeutics 2010; 7: 115–26.

Mendoza-Fernandez V, Andrew RD, Barajas-Lopez C. ATP inhibits glutamate synaptic release by acting at P2Y receptors in pyramidal neurons of hippocampal slices. J Pharmacol Exp Ther 2000; 293: 172–9.

Myer DJ, Gurkoff GG, Lee SM, Hovda DA, Sofroniew MV. Essential protective roles of reactive astrocytes in traumatic brain injury. Brain 2006; 129: 2761–72.

Neary JT, Kang Y, Willoughby KA, Ellis EF. Activation of extracellular signal-regulated kinase by stretch-induced injury in astrocytes involves extracellular ATP and P2 purinergic receptors. J Neurosci 2003; 23: 2348–56.

Nedergaard M, Ransom B, Goldman SA. New roles for astrocytes: redefining the functional architecture of the brain. Trends Neurosci 2003; 26: 523–30.

Newman EA. Propagation of intercellular calcium waves in retinal astrocytes and Muller cells. J Neurosci 2001; 21: 2215–23.

Oliveira-da-Silva A, Manhaes AC, Cristina-Rodrigues F, Filgueiras CC, Abreu-Villaca Y. Hippocampal increased cell death and decreased cell density elicited by nicotine and/or ethanol during adolescence are reversed during drug withdrawal. Neuroscience 2010; 167: 163–73.

Parpura V, Basarsky TA, Liu F, Jeftinija K, Jeftinija S, Haydon PG. Glutamate-mediated astrocyte-neuron signalling. Nature 1994; 369: 744–7.

Pascual O, Casper KB, Kubera C, Zhang J, Revilla-Sanchez R, Sul JY, et al. Astrocytic purinergic signaling coordinates synaptic networks. Science 2005; 310: 113–16.

Peden M, Scurfield R, Sleet D, Mohan D, Hyder AA, Jarawan E, et al. World report on road traffic injury prevention. Geneva, 2004.

Risdall JE, Menon DK. Traumatic brain injury. Philos Trans R Soc Lond B Biol Sci 2011; 366: 241–50.

Rodrigues RJ, Almeida T, Richardson PJ, Oliveira CR, Cunha RA. Dual presynaptic control by ATP of glutamate release via facilitatory P2X1, P2X2/3, and P2X3 and inhibitory P2Y1, P2Y2, and/or P2Y4 receptors in the rat hippocampus. J Neurosci 2005; 25: 6286–95.

Rodriguez-Zayas AE, Torrado AI, Rosas OR, Santiago JM, Figueroa JD, Miranda JD. Blockade of p2 nucleotide receptors after spinal cord injury reduced the gliotic response and spared tissue. J Mol Neurosci 2012; 46: 167–76.

Rzigalinski BA, Weber JT, Willoughby KA, Ellis EF. Intracellular free calcium dynamics in stretch-injured astrocytes. J Neurochem 1998; 70: 2377–85.

Shreiber DI, Smith DH, Meaney DF. Immediate in vivo response of the cortex and the blood-brain barrier following dynamic cortical deformation in the rat. Neurosci Lett 1999; 259: 5–8.

Smith DH, Soares HD, Pierce JS, Perlman KG, Saatman KE, Meaney DF, et al. A model of parasagittal controlled cortical impact in the mouse: cognitive and histopathologic effects. J Neurotrauma 1995; 12: 169–78.

Starkov AA, Chinopoulos C, Fiskum G. Mitochondrial calcium and oxidative stress as mediators of ischemic brain injury. Cell Calcium 2004; 36: 257–64.

Tian GF, Takano T, Lin JH, Wang X, Bekar L, Nedergaard M. Imaging of cortical astrocytes using 2-photon laser scanning microscopy in the intact mouse brain. Adv Drug Deliv Rev 2006; 58: 773–87.

Tonazzini I, Trincavelli ML, Storm-Mathisen J, Martini C, Bergersen LH. Co-localization and functional cross-talk between A1 and P2Y1 purine receptors in rat hippocampus. Eur J Neurosci 2007; 26: 890–902.

Van Den Heuvel C, Thornton E, Vink R. Traumatic brain injury and Alzheimer's disease: a review. In: Weber JT, Maas AIR, editors. Neurotrauma: new insights into pathology and treatment. Vol. Vol. 161. Amsterdam: Elsevier Science Bv; 2007. p. 303–16.

Venance L, Stella N, Glowinski J, Giaume C. Mechanism involved in initiation and propagation of receptor-induced intercellular calcium signaling in cultured rat astrocytes. J Neurosci 1997; 17: 1981–92.

Ventura R, Harris KM. Three-dimensional relationships between hippocampal synapses and astrocytes. J Neurosci 1999; 19: 6897–906.

Wu LG, Saggau P. Adenosine inhibits evoked synaptic transmission primarily by reducing presynaptic calcium influx in area CA1 of hippocampus. Neuron 1994; 12: 1139–48.

Yiu G, He Z. Glial inhibition of CNS axon regeneration. Nat Rev Neurosci 2006; 7: 617–27.

Yuste R, Peinado A, Katz LC. Neuronal domains in developing neocortex. Science 1992; 257: 665–9.